The Astrophysical Journal, 944:166 (9pp), 2023 February 20 https://doi.org/10.3847/1538-4357/acafdd

Search for Gamma-Ray and Neutrino Coincidences Using HAWC and ANTARES Data

H. A. Ayala Solares[1], S. Coutu[1], D. Cowen[1], D. B. Fox[1], T. Grégoire[1], F. McBride[2], M. Mostafá[1], K. Murase[1], S. Wissel[1]
AMON Team,
A. Albert[3,4], S. Alves[5], M. André[6], M. Ardid[7], S. Ardid[7], J.-J. Aubert[8], J. Aublin[9], B. Baret[9], S. Basa[10], B. Belhorma[11], M. Bendahman[9,12], F. Benfenati[13,14], V. Bertin[8], S. Biagi[15], M. Bissinger[16], J. Boumaaza[12], M. Bouta[17], M. C. Bouwhuis[18], H. Brânzaş[19], R. Bruijn[18,20], J. Brunner[8], J. Busto[8], B. Caiffi[21], D. Calvo[5], A. Capone[22,23], L. Caramete[19], J. Carr[8], V. Carretero[5], S. Celli[22,23], M. Chabab[24], T. N. Chau[9], R. Cherkaoui El Moursli[12], T. Chiarusi[13], M. Circella[25], J. A. B. Coelho[9], A. Coleiro[9], R. Coniglione[15], P. Coyle[8], A. Creusot[9], A. F. Díaz[26], G. de Wasseige[9], B. De Martino[8], C. Distefano[15], I. Di Palma[22,23], A. Domi[18,20], C. Donzaud[9,27], D. Dornic[8], D. Drouhin[3,4], T. Eberl[16], T. van Eeden[18], D. van Eijk[18], N. El Khayati[12], A. Enzenhöfer[8], P. Fermani[22,23], G. Ferrara[15], F. Filippini[13,14], L. Fusco[28], J. García[7], P. Gay[9,29], H. Glotin[30], R. Gozzini[5], R. Gracia Ruiz[18], K. Graf[16], C. Guidi[21,31], S. Hallmann[16], H. van Haren[32], A. J. Heijboer[18], Y. Hello[33], J. J. Hernández-Rey[5], J. Hößl[16], J. Hofestädt[16], F. Huang[8], G. Illuminati[13,14], C. W. James[34], B. Jisse-Jung[18], M. de Jong[18,35], P. de Jong[18,20], M. Kadler[36], O. Kalekin[16], U. Katz[16], A. Kouchner[9], I. Kreykenbohm[37], V. Kulikovskiy[21], R. Lahmann[16], M. Lamoureux[9], R. Le Breton[9], D. Lefèvre[38,39], E. Leonora[40], G. Levi[13,14], S. Le Stum[8], D. Lopez-Coto[41], S. Loucatos[9,42], L. Maderer[9], J. Manczak[5], M. Marcelin[10], A. Margiotta[13,14], A. Marinelli[43], J. A. Martínez-Mora[7], K. Melis[18,20], P. Migliozzi[43], A. Moussa[17], R. Muller[18], L. Nauta[18], S. Navas[41], E. Nezri[10], B. Ó Fearraigh[18], A. Păun[19], G. E. Păvălaş[19], C. Pellegrino[13,44,45], M. Perrin-Terrin[8], V. Pestel[18], P. Piattelli[15], C. Pieterse[5], C. Poirè[7], V. Popa[19], T. Pradier[3], N. Randazzo[40], D. Real[5], S. Reck[16], G. Riccobene[15], A. Romanov[21,31], A. Sánchez-Losa[5,25], D. F. E. Samtleben[18,35], M. Sanguineti[21,31], P. Sapienza[15], J. Schnabel[16], J. Schumann[16], F. Schüssler[42], J. Seneca[18], M. Spurio[13,14], Th. Stolarczyk[42], M. Taiuti[21,31], Y. Tayalati[12], S. J. Tingay[34], B. Vallage[9,42], V. Van Elewyck[9,46], F. Versari[9,13,14], S. Viola[15], D. Vivolo[43,47], J. Wilms[37], S. Zavatarelli[21], A. Zegarelli[22,23], J. D. Zornoza[5], J. Zúñiga[5]
ANTARES Collaboration,
and
A. Albert[48], C. Alvarez[49], J. C. Arteaga-Velázquez[50], R. Babu[51], E. Belmont-Moreno[52], K. S. Caballero-Mora[49], T. Capistrán[53], A. Carramiñana[54], S. Casanova[55], U. Cotti[50], O. Chaparro-Amaro[56], J. Cotzomi[57], S. Coutiño de León[58], E. De la Fuente[59], C. de León[50], R. Diaz Hernandez[54], M. A. DuVernois[58], M. Durocher[48], J. C. Díaz-Vélez[59], K. Engel[60], C. Espinoza[52], K. L. Fan[60], M. Fernández Alonso[1,61], N. Fraija[53], J. A. García-González[62], F. Garfias[53], M. M. González[53], J. A. Goodman[60], J. P. Harding[48], S. Hernandez[52], D. Huang[51], F. Hueyotl-Zahuantitla[49], P. Hüntemeyer[51], A. Iriarte[53], V. Joshi[63], S. Kaufmann[64], A. Lara[65], H. León Vargas[52], J. T. Linnemann[66], A. L. Longinotti[53], G. Luis-Raya[64], K. Malone[67], O. Martinez[57], I. Martinez-Castellanos[60], J. Martínez-Castro[56], J. A. Matthews[68], P. Miranda-Romagnoli[69], J. A. Morales-Soto[50], E. Moreno[57], A. Nayerhoda[55], L. Nellen[70], M. U. Nisa[66], R. Noriega-Papaqui[69], N. Omodei[71], A. Peisker[66], Y. Pérez Araujo[53], E. G. Pérez-Pérez[64], C. D. Rho[72], D. Rosa-González[54], E. Ruiz-Velasco[73], H. Salazar[74], F. Salesa Greus[5,55], A. Sandoval[52], M. Schneider[60], A. J. Smith[60], Y. Son[72], R. W. Springer[75], O. Tibolla[76], K. Tollefson[66], I. Torres[54], R. Torres-Escobedo[77], R. Turner[51], F. Ureña-Mena[54], E. Varela[57], X. Wang[51], K. Whitaker[1], E. Willox[60], A. Zepeda[78], and H. Zhou[77]
HAWC Collaboration
[1] Department of Physics, Pennsylvania State University, University Park, PA 16802, USA; hgayala@psu.edu
[2] Department of Physics and Astronomy, Bowdoin College, Brunswick, ME 04011, USA
[3] Université de Strasbourg, CNRS, IPHC UMR 7178, F-67000 Strasbourg, France
[4] Université de Haute Alsace, F-68100 Mulhouse, France
[5] IFIC—Instituto de Física Corpuscular (CSIC—Universitat de València) c/ Catedrático José Beltrán, 2 E-46980 Paterna, Valencia, Spain
[6] Technical University of Catalonia, Laboratory of Applied Bioacoustics, Rambla Exposició, E-08800 Vilanova i la Geltrú, Barcelona, Spain
[7] Institut d'Investigació per a la Gestió Integrada de les Zones Costaneres (IGIC) - Universitat Politècnica de València. C/ Paranimf 1, E-46730 Gandia, Spain
[8] Aix Marseille Univ, CNRS/IN2P3, CPPM, Marseille, France
[9] Université de Paris, CNRS, Astroparticule et Cosmologie, F-75013 Paris, France
[10] Aix Marseille Univ, CNRS, CNES, LAM, Marseille, France
[11] National Center for Energy Sciences and Nuclear Techniques, B.P.1382, R.P.10001 Rabat, Morocco
[12] University Mohammed V in Rabat, Faculty of Sciences, 4 av. Ibn Battouta, B.P. 1014, R.P. 10000 Rabat, Morocco
[13] INFN—Sezione di Bologna, Viale Berti-Pichat 6/2, I-40127 Bologna, Italy
[14] Dipartimento di Fisica e Astronomia dell'Università, Viale Berti Pichat 6/2, I-40127 Bologna, Italy
[15] INFN—Laboratori Nazionali del Sud (LNS), Via S. Sofia 62, I-95123 Catania, Italy
[16] Friedrich-Alexander-Universität Erlangen-Nürnberg, Erlangen Centre for Astroparticle Physics, Erwin-Rommel-Str. 1, D-91058 Erlangen, Germany
[17] University Mohammed I, Laboratory of Physics of Matter and Radiations, B.P.717, Oujda 6000, Morocco
[18] Nikhef, Science Park, Amsterdam, The Netherlands
[19] Institute of Space Science, RO-077125 Bucharest, Măgurele, Romania
[20] Universiteit van Amsterdam, Instituut voor Hoge-Energie Fysica, Science Park 105, 1098 XG Amsterdam, The Netherlands
[21] INFN—Sezione di Genova, Via Dodecaneso 33, I-16146 Genova, Italy

[22] INFN—Sezione di Roma, P.le Aldo Moro 2, I-00185 Roma, Italy
[23] Dipartimento di Fisica dell'Università La Sapienza, P.le Aldo Moro 2, I-00185 Roma, Italy
[24] LPHEA, Faculty of Science—Semlali, Cadi Ayyad University, P.O.B. 2390, Marrakech, Morocco
[25] INFN—Sezione di Bari, Via E. Orabona 4, I-70126 Bari, Italy
[26] Department of Computer Architecture and Technology/CITIC, University of Granada, E-18071 Granada, Spain
[27] Université Paris-Sud, F-91405 Orsay Cedex, France
[28] Università di Salerno e INFN Gruppo Collegato di Salerno, Dipartimento di Fisica, Via Giovanni Paolo II 132, Fisciano, I-84084 Italy
[29] Laboratoire de Physique Corpusculaire, Clermont Université, Université Blaise Pascal, CNRS/IN2P3, BP 10448, F-63000 Clermont-Ferrand, France
[30] LIS, UMR Université de Toulon, Aix Marseille Université, CNRS, F-83041 Toulon, France
[31] Dipartimento di Fisica dell'Università, Via Dodecaneso 33, I-16146 Genova, Italy
[32] Royal Netherlands Institute for Sea Research (NIOZ), Landsdiep 4, 1797 SZ 't Horntje (Texel), The Netherlands
[33] Géoazur, UCA, CNRS, IRD, Observatoire de la Côte d'Azur, Sophia Antipolis, France
[34] International Centre for Radio Astronomy Research—Curtin University, Bentley, WA 6102, Australia
[35] Huygens-Kamerlingh Onnes Laboratorium, Universiteit Leiden, The Netherlands
[36] Institut für Theoretische Physik und Astrophysik, Universität Würzburg, Emil-Fischer Str. 31, D-97074 Würzburg, Germany
[37] Dr. Remeis-Sternwarte and ECAP, Friedrich-Alexander-Universität Erlangen-Nürnberg, Sternwartstr. 7, D-96049 Bamberg, Germany
[38] Mediterranean Institute of Oceanography (MIO), Aix-Marseille University, F-13288, Marseille, Cedex 9, France
[39] Université du Sud Toulon-Var, CNRS-INSU/IRD UM 110, F-83957, La Garde Cedex, France
[40] INFN—Sezione di Catania, Via S. Sofia 64, I-95123 Catania, Italy
[41] Dpto. de Física Teórica y del Cosmos & C.A.F.P.E., University of Granada, 18071 Granada, Spain
[42] IRFU, CEA, Université Paris-Saclay, F-91191 Gif-sur-Yvette, France
[43] INFN—Sezione di Napoli, Via Cintia I-80126, Napoli, Italy
[44] Museo Storico della Fisica e Centro Studi e Ricerche Enrico Fermi, Piazza del Viminale 1, 00184, Roma, Italy
[45] INFN—CNAF, Viale C. Berti Pichat 6/2, 40127, Bologna, Italy
[46] Institut Universitaire de France, F-75005 Paris, France
[47] Dipartimento di Fisica dell'Università Federico II di Napoli, Via Cintia I-80126, Napoli, Italy
[48] Physics Division, Los Alamos National Laboratory, Los Alamos, NM, USA
[49] Universidad Autónoma de Chiapas, Tuxtla Gutiérrez, Chiapas, México
[50] Universidad Michoacana de San Nicolás de Hidalgo, Morelia, México
[51] Department of Physics, Michigan Technological University, Houghton, MI, USA
[52] Instituto de Física, Universidad Nacional Autónoma de México, Ciudad de México, México
[53] Instituto de Astronomía, Universidad Nacional Autónoma de México, Ciudad de México, México
[54] Instituto Nacional de Astrofísica, Óptica y Electrónica, Puebla, México
[55] Institute of Nuclear Physics Polish Academy of Sciences, PL-31342 IFJ-PAN, Krakow, Poland
[56] Centro de Investigación en Computación, Instituto Politécnico Nacional, Mexico City, Mexico
[57] Facultad de Ciencias Físico Matemácas, Benemérita Universidad Autónoma de Puebla, Puebla, México
[58] Department of Physics, University of Wisconsin-Madison, Madison, WI 53706, USA
[59] Departamento de Física, Centro Universitario de Ciencias Exactas e Ingenierias, Universidad de Guadalajara, Guadalajara, México
[60] Dept. of Physics, University of Maryland, College Park, MD 20742, USA
[61] Gran Sasso Science Institute (GSSI), Via Iacobucci 2, I–67100 L′Aquila, Italy AND Istituto Nazionale di Fisica Nucleare (INFN)–Laboratori Nazionali del Gran Sasso, I–67100 Assergi, L′Aquila, Italy
[62] Tecnologico de Monterrey, Escuela de Ingeniería y Ciencias, Ave. Eugenio Garza Sada 2501, Monterrey, N.L., Mexico
[63] Erlangen Centre for Astroparticle Physics, Friedrich-Alexander-Universität Erlangen-Nürnberg, D-91058 Erlangen, Germany
[64] Universidad Politecnica de Pachuca, Pachuca, Hgo, México
[65] Instituto de Geofísica, Universidad Nacional Autónoma de México, Ciudad de México, México
[66] Dept. of Physics and Astronomy, Michigan State University, East Lansing, MI 48824, USA
[67] Space Science and Applications Group, Los Alamos National Laboratory, Los Alamos, NM, USA
[68] Dept of Physics and Astronomy, University of New Mexico, Albuquerque, NM, USA
[69] Universidad Autónoma del Estado de Hidalgo, Pachuca, México
[70] Instituto de Ciencias Nucleares, Universidad Nacional Autónoma de México, Ciudad de México, México
[71] Department of Physics, Stanford University, Stanford, CA 94305-4060, USA
[72] Natural Science Research Institute, University of Seoul, Seoul, Republic Of Korea
[73] Max-Planck Institute for Nuclear Physics, D-69117 Heidelberg, Germany
[74] Facultad de Ciencias Físico Matemáticas, Benemérita Universidad Autónoma de Puebla, Puebla, México
[75] Department of Physics and Astronomy, University of Utah, Salt Lake City, UT, USA
[76] Universidad Politecnica de Pachuca, Pachuca, Mexico
[77] Tsung-Dao Lee Institute & School of Physics and Astronomy, Shanghai Jiao Tong University, Shanghai, People's Republic of China
[78] Physics Department, Centro de Investigacion y de Estudios Avanzados del IPN, Mexico City, DF, Mexico
Received 2022 September 27; revised 2022 December 1; accepted 2022 December 22; published 2023 February 22

Abstract

In the quest for high-energy neutrino sources, the Astrophysical Multimessenger Observatory Network has implemented a new search by combining data from the High Altitude Water Cherenkov (HAWC) Observatory and the Astronomy with a Neutrino Telescope and Abyss environmental RESearch (ANTARES) neutrino telescope. Using the same analysis strategy as in a previous detector combination of HAWC and IceCube data, we perform a search for coincidences in HAWC and ANTARES events that are below the threshold for sending public alerts in each individual detector. Data were collected between 2015 July and 2020 February with a live time of 4.39 yr. Over this time period, three coincident events with an estimated false-alarm rate of <1 coincidence per year were

found. This number is consistent with background expectations.

Unified Astronomy Thesaurus concepts: High energy astrophysics (739)

1. Introduction

The Astrophysical Multimessenger Observatory Network (AMON; Ayala Solares et al. 2020) is a virtual hub that integrates heterogeneous data from different astrophysical observatories with the main objective of enabling multi-messenger astrophysics. Observatories that become members of AMON can act as trigger observatories or as follow-up observatories. Trigger observatories have high-duty cycles and a large field of view. Follow-up observatories have better angular resolution and sensitivity. AMON has developed coincidence analyses between high-energy gamma-ray and high-energy neutrino data. AMON mainly, but not necessarily, receives and uses data that are below the astrophysical-event selection threshold (called subthreshold) for the individual observatories. In these data, possible signal events of astrophysical origin can be present and due to the limited sensitivity of a given detector (e.g., HAWC or ANTARES), cannot be distinguished from background events. Using a statistical analysis, AMON looks for temporal and/or spatial coincidences between events collected by different observatories with the purpose of recovering the signal events that are buried in the background.

The AMON analyses using gamma-ray and neutrino data include the coincidence studies between IceCube and Fermi-LAT (Turley et al. 2018); ANTARES and Fermi-LAT (Ayala Solares et al. 2019); and HAWC and IceCube (Ayala Solares et al. 2021). The last two analyses make use of the Neutrino-Electromagnetic (NuEM) AMON channel. This channel generates alerts in real time after receiving data from the respective observatories and performing a calculation to rank the coincidences (see Section 3). AMON servers are now located at the Amazon Web Services, having a high up-time (>99.99%). The NuEM alerts are sent as notices and circulars to the Gamma-ray Coordinates Network.[79] Recently, AMON also started to send alerts to the Scalable Cyberinfrastructure to support Multi-Messenger Astrophysics[80] (Chang et al. 2019), a new hub for multimessenger astrophysics designed for private and public communication.

The NuEM channel searches for sources that emit secondary neutrinos and gamma rays. These neutrinos and gamma rays are produced in hadronic interactions, such as inelastic collisions of cosmic rays with matter or with radiation fields. These hadronic interactions produce neutral and charged pions, which then decay into the aforementioned particles. These interactions can occur in a wide variety of sources such as blazar flares, tidal disruption events, long gamma-ray bursts, short gamma-ray bursts, supernovae, and compact binary mergers (for a review of multimessenger sources, see Murase & Bartos 2019). In this work, we present a new analysis of this channel: the coincidence search between events collected by the HAWC gamma-ray observatory and the ANTARES neutrino telescope.

With ANTARES recently ceasing operations, this analysis helps us not only to look for possible sources in existing data but also to prepare the necessary analysis tools and infrastructure for the KM3NeT neutrino telescope (Adrián-Martínez et al. 2016), the successor of ANTARES.

[79] https://gcn.gsfc.nasa.gov/

[80] https://scimma.org/index.html

2. HAWC and ANTARES: Detectors and Data Sets

2.1. HAWC

The HAWC Observatory monitors the gamma-ray sky from its location in Puebla, Mexico, at an altitude of 4100 meters above sea level. Sitting between the volcanoes Sierra Negra and Pico de Orizaba, it has a large field of view that covers two-thirds of the sky daily. With a duty cycle above 95%, HAWC can monitor 2 sr of the sky continuously, which makes it ideal for observing transient events (Abeysekara et al. 2017). HAWC is a water Cherenkov detector array that characterizes the footprints of extensive air showers on the ground. Hadron-like showers and gamma-like showers can then be classified by how smooth and compact the distribution of the charge measured by the photomultiplier tubes (PMTs) is in the array. Hadron-like showers tend to have a discontinuous profile on the array due to the large number of muons in the shower, while gamma-ray showers present a smoother profile. By using the trigger time information of each PMT, reconstruction algorithms can find the direction of the primary particle with a 68% resolution of $\sim 0.^{\circ}2$ at energies above 10 TeV. HAWC is sensitive to gamma rays with energy from 300 GeV up to >100 TeV (Abeysekara et al. 2017; Albert et al. 2020).

The data that AMON receives from HAWC for this analysis includes the rising and setting times of the event position in the sky with respect to the detector—which defines the "HAWC transit time" of the event; a parameter (referred to as the "significance value" in the rest of the article) that estimates how much the event deviates from the expected hadron-like background and is calculated after one transit; and the position in the sky of every event with their uncertainty. HAWC events are referred as "hotspots." The data used in this work were collected from 2015 July to 2020 February.

2.2. ANTARES

The ANTARES neutrino telescope (Ageron et al. 2011) is located 40 km offshore from the city of Toulon, France, in the Mediterranean Sea. It is a deep-sea Cherenkov neutrino detector. The detector consists of a three-dimensional array of 885 optical modules, each one with a 10 inch PMT, and distributed over 12 vertical strings anchored in the seafloor at a depth of about 2400 m. The detection of light from up-going charged particles is optimized with the PMTs facing 45° downward. Since 2007 May, the telescope has detected neutrino-induced muons that cause the emission of Cherenkov light in the detector, producing track-like events. Charged-current interactions induced by electron neutrinos (and possibly, by tau neutrinos of cosmic origin) or neutral-current interactions of all neutrino flavors can be reconstructed as cascade-like events (Albert et al. 2017). For the analysis presented in this manuscript, we use track-like events that are used in the point-source search analysis of ANTARES (Illuminati et al. 2019), which have a median angular resolution of $0.^{\circ}4$ for energies above 10 TeV. Since the ANTARES data

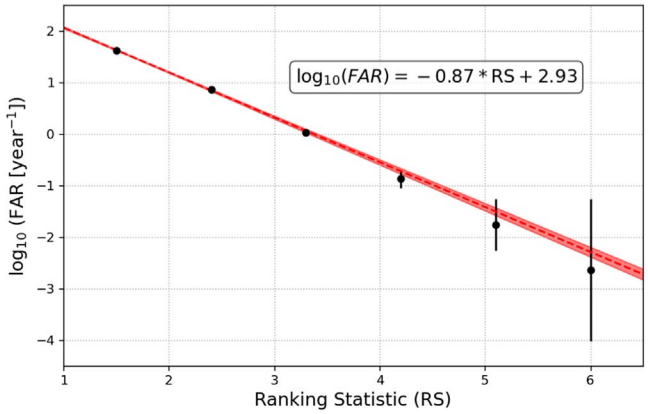

Figure 1. FAR of the analysis. The result and equation of the linear fit, together with the 1σ statistical band, are also shown.

are public, we are not using subthreshold data from ANTARES for this analysis.

The ANTARES data information consists of the following: the position and uncertainty of the individual observed event, the time of the event, and a p-value that quantifies the probability of the event to be a background event. For this study, we use the archival public data (2007–2017) that can be found in Albert et al. (2018) as well as 3 more years of archival data (up to 2020) given by ANTARES through the AMON memorandum of understanding. Since we are using the ANTARES public data, they do not contain subthreshold events. We use the data that overlap with the time period of the HAWC data.

3. The Coincidence Analysis

3.1. Computing the Ranking Statistic

The analysis method applied in this work is the same as the one developed for the HAWC and IceCube detectors in Ayala Solares et al. (2021), which is summarized below.

We assume to have a coincidence when the time of the ANTARES event falls between the rising and setting times of the HAWC event and the distance between the reconstructed directions of the events is smaller than 3°.5 (same as in Ayala Solares et al. 2021). After finding a coincidence, a test statistic is calculated to rank the coincidence. This is defined as

$$\chi^2_{6+2n_\nu} = -2\ln(p_\lambda p_{\rm HAWC} p_{\rm Cluster} \prod_i^{n_\nu} p_{{\rm ANTARES},i}), \quad (1)$$

which is based on Fisher's method (Fisher 1938). The number of degrees of freedom of the test statistic is twice the number of p-values. The p_λ value measures how much the events spatially overlap with each other. This value is obtained after optimizing a log-likelihood function defined as

$$\lambda(\boldsymbol{x}) = \sum_{i=1}^{N} \ln \frac{S_i(\boldsymbol{x})}{B_i}. \quad (2)$$

Here $S_i(\boldsymbol{x}) = \exp[-(\boldsymbol{x} - \boldsymbol{x}_i)^2/2\sigma_i^2]/(2\pi\sigma_i^2)$, a 2D Gaussian on a sphere with $\boldsymbol{x}_i$ and σ_i being the measured position and positional uncertainty of the ith event. B_i is the background directional probability distribution from the corresponding detector at the position of the events. The sum is over all the N events that are part of the coincidence. The position of the coincidence, $\boldsymbol{x}_{\rm coinc}$, is defined as the position where the log-likelihood is maximized, $\lambda_{\rm max}$. The p_λ is obtained from the $\lambda_{\rm max}$ distribution, which is the probability of seeing a $\lambda_{\rm max}$ or higher.

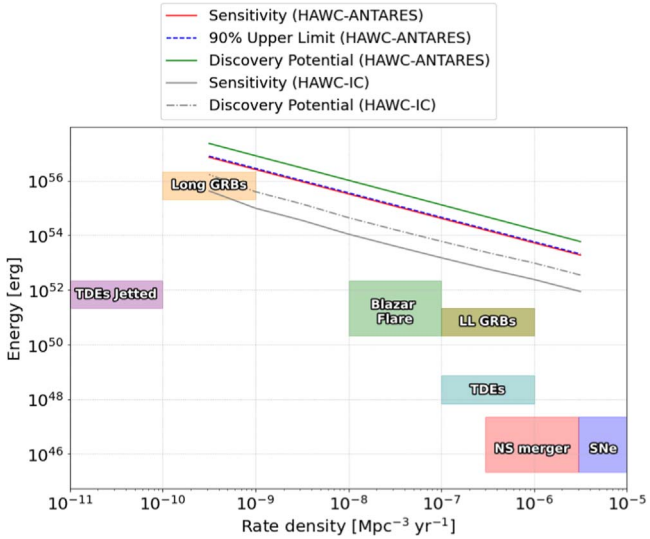

Figure 2. Sensitivity, discovery potential (5σ), and 90% upper limit for the archival data (analysis live time of 4.39 yr) in terms of total isotropic equivalent neutrino energy as a function of the local rate density. We assume a burst time of 6 hr and the neutrino spectrum to be a power law with index −2.0. Luminosity and rate-density ranges of the different sources can be found in Murase & Bartos (2019). For comparison, we show the sensitivity and discovery potential of the HAWC-IceCube analysis from Ayala Solares et al. (2021). Both the ANTARES effective area and the overlap region between HAWC and ANTARES are smaller compared to those in the HAWC-IceCube analysis. We can see that long gamma-ray bursts are potential candidates for a possible coincidence detection.

The $p_{\rm HAWC}$ value is related to the significance value of the HAWC event and quantifies the probability for the event to be from the background.

The $p_{\rm Cluster}$ is the probability of having n_ν ANTARES events when one is already observed. It is defined as

$$p_{{\rm Cluster}(n_\nu)} = 1 - \sum_{i=0}^{n_\nu - 2} {\rm Poisson}(i; f_\nu \Delta t), \quad (3)$$

where Δt is the HAWC transit time; f_ν is the ANTARES background rate in a 3°.5 circle in the sky estimated as $f_\nu = f_{\rm all}\frac{\Omega}{4\pi} = f_{\rm all}(1 - \cos(3^\circ.5))/2$, where $f_{\rm all}$ is the measured background rate from the whole sky.

Finally, $p_{{\rm ANTARES},i}$ is the fraction of ANTARES events that has a larger number of hits in the detector than the observed number of hits for the event. It is computed by using the normalized anticumulative distribution of the number of hits from the full ANTARES public data.

Since there can be n_ν ANTARES events passing the selection criteria during a HAWC time window, the degrees of freedom of Equation (1) vary. Therefore, we compute the p-value of the $\chi^2_{6+2n_\nu}$ with $6+2n_\nu$ degrees of freedom. The ranking statistic (RS) is then simply defined as

$${\rm RS} = -\log_{10}(p\text{-value}_{\chi^2_{6+2n_\nu}}). \quad (4)$$

3.2. Calculating the False-alarm Rate

The distribution of the RS is used to quantify the probability that the coincidences are fortuitous. It is also used to calculate the false-alarm rate (FAR) of the coincidence (i.e., how rare the RS is). To build the distribution, we perform several simulations

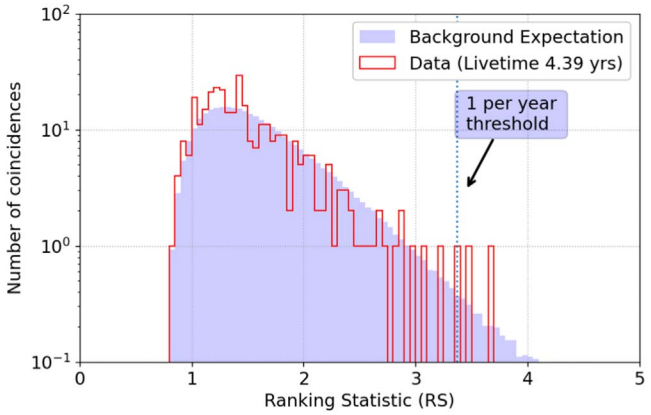

Figure 3. RS distribution of the analysis. Blue: expected distribution obtained from the scrambled data set and normalized to the number of coincidences observed in the data set. Red: distribution of the unscrambled data. The vertical line marks the 1-per-year FAR coincidence threshold.

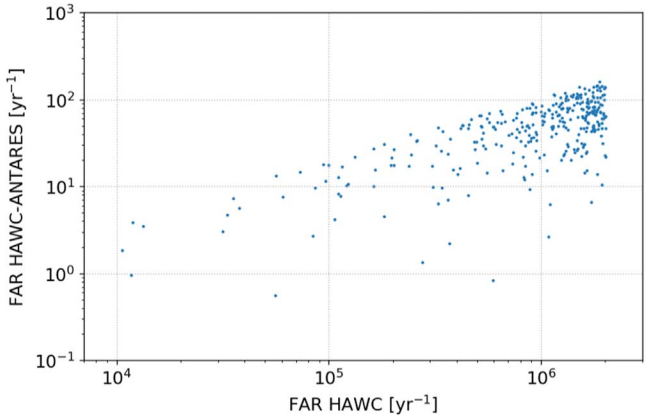

Figure 4. Comparison of the FAR of the coincidence analysis vs. the FAR of HAWC alone. The combined analysis reduces by several orders of magnitude the FAR of the events.

by scrambling the data sets a thousand times. The scrambling consists of randomizing the R.A. and the time values of the events. We then count how many events are above an RS value and divide by the simulated time (∼4600 yr). Figure 1 shows the FAR as a function of the RS. A red line is shown that fits the data points, together with the 1σ uncertainty band.

3.3. Sensitivity and Discovery Potential

We obtain the sensitivity and discovery potential in the parameter space composed of the local rate density of transient sources versus the total neutrino isotropic energy as in Ayala Solares et al. (2021). We compare this to different source populations. We use the FIRESONG software package (Taboada et al. 2017) to obtain the number of transient sources during the same time as the archival data, along with the redshift, the neutrino flux normalization, and the position in the sky of each source. The star formation rate assumed is from the core-collapse supernova rate obtained from the CANDELS and CLASH supernova surveys (Strolger et al. 2015). We assume a local rate density and a total neutrino isotropic equivalent energy as denoted along the x- and y-axes of Figure 2. The duration of each burst is fixed to 6 hr. For the neutrino energy spectrum, we assume a power law with a spectral index of -2.0 in the energy range between 10 TeV and 10 PeV. We use the

Table 1
Summary Information for the Three Coincidences with FAR <1 yr^{-1}

Coincidence ID	Decl. (deg)	R.A. (deg)	U_C (50%) (deg)	RS	FAR [yr^{-1}]	p-value
1	25.0	25.6	0.18	3.46	0.83	0.97
2	−0.8	222.7	0.16	3.38	0.96	0.98
3	3.4	85.4	0.16	3.65	0.56	0.91

Note. Information for the HAWC and ANTARES events that make these coincidences are found in Tables 2 and 3. The coincidence positions and uncertainty circles are shown as red in the sky maps of Figure 5. The uncertainty $U_C(50\%)$ corresponds to the 50% containment region of the estimated position of the coincidence. RS is the ranking statistic as defined in Section 3.1. The p-value corresponds to the posttrial p-value.

model from Ahlers & Murase (2014) given as

$$E_\gamma F_\gamma(E_\gamma) \approx e^{-\frac{d}{\lambda_{\gamma\gamma}}} \frac{2}{3K} \sum_{\nu_\alpha} E_\nu F_{\nu_\alpha}(E_\nu), \quad (5)$$

where d is the distance to the source; $\lambda_{\gamma\gamma}$ is the interaction length of gamma rays with radiation backgrounds; $K = 1$ for photohadronic interactions, and $K = 2$ for hadro-nuclear interactions; and the sum is over the neutrino flavors. Using the neutrino flux normalization, and assuming photohadronic interactions, we can obtain the gamma-ray flux normalization from Equation (5).[81]

After obtaining the gamma-ray flux normalization, we inject the sources in HAWC simulated data. Using the simulated redshift information, we apply the attenuation of gamma rays from the extragalactic background light using the model from Domínguez et al. (2011). After running the HAWC analysis, if the observed hotspot has a significance larger than 2.75σ, we proceed to inject the neutrinos using Monte Carlo signal data from the ANTARES simulation as well as background events from the ANTARES scrambled data sets. Then we proceed to calculate the RS as explained in Section 3.1. We simulate transient sources for a period with the same live time as the archival data being used in this analysis.

To be able to estimate the sensitivity and discovery potential, we use the number of coincidences above the 1-per-year threshold as a statistic. For the live time of the analysis, we expect to observe at least ∼44 random coincidences. Using random samples from the RS distribution, we find that the distribution of the number of coincidences behaves as a Poisson distribution with a mean of $\lambda_{\rm bk} = 4.39$ since that is the live time of the analysis. We now need to find limits on the total signal and background rate, $\lambda_{\rm bk} + \lambda_{\rm s}$. In order to obtain the sensitivity, we need a total rate that will produce a Poisson distribution with 90% of its population above the median of the background Poisson distribution. For the discovery potential, we need a total rate that will produce a Poisson distribution with 50% of its population above the threshold of the p-value $= 2.87 \times 10^{-7}$ (5σ) of the background distribution. The mean signal $\lambda_{\rm s}$ values for the sensitivity and discovery potential are 3.6 and 14.3.

[81] For our estimation, and to compare with the result from Ayala Solares et al. (2021), we assume an equal ratio of neutrino flavors when detected. This makes all three flavor fluxes similar, and hence the factor of $1/3$ is canceled. Since $E_\gamma \approx 2E_\nu$, we end up with $F_\gamma(E_\gamma) \approx F_\nu(E_\nu)$ at location $d = 0$. The gamma-ray flux is then attenuated as mentioned in the main text.

Table 2
Information on the HAWC "hotspots" that Correspond to Each of the Coincidences with a FAR $< 1\ \mathrm{yr}^{-1}$

Dec (deg)	RA (deg)	$U_H(50\%)$ (deg)	Rising Time (UT)	Setting Time (UT)	Significance σ	Flux $\times 10^{-11}[\mathrm{TeV}^{-1}\ \mathrm{cm}^{-2}\ \mathrm{s}^{-1}]$	Spectral Index
25.2	25.7	0.20	2016-01-07 21:29:40	2016-01-08 04:39:38	3.18	2.0 ± 0.8	2.5
−0.8	222.4	0.20	2017-09-06 19:08:16	2017-09-07 01:21:22	4.29	5.0 ± 1.6	2.5
3.4	85.7	0.17	2019-03-28 20:33:04	2019-03-29 03:01:18	3.89	4.9 ± 1.6	3.0

Note. The positions and uncertainty circles of the HAWC "hotspots" are shown as blue in the sky maps of Figure 5. The uncertainty $U_H(50\%)$ corresponds to the 50% containment region of the HAWC hotspot. The assumed flux model is a power law with an index shown in the last column. The index is fixed during the fit. The flux measurement is the normalization of the power law at 1 TeV.

Table 3
ANTARES Event Information for Each Coincidence

Dec (deg)	RA (deg)	$U_A(50\%)$ (deg)	Time (UT)	Background p-value	$\Delta\theta$ (deg)
24.1	25.4	0.45	2016-01-08 04:24:40.32	0.009	1.10
−0.5	225.6	0.47	2017-09-06 22:10:24.96	0.095	3.28
3.4	85.6	0.36	2019-03-29 01:03:47.0	0.51	0.33

Note. The positions and uncertainty circles of the ANTARES events are shown as filled black circles in the sky maps of Figure 5. The uncertainty $U_A(50\%)$ corresponds to the 50% containment region of the ANTARES position. $\Delta\theta$ is the distance from the best-fit HAWC hotspot position to the measured ANTARES event position.

We perform the simulation 100 times for each pair of local rate density of transient sources and total isotropic equivalent energies to gather enough statistics to build the Poisson distributions. The value of the rate densities and isotropic energies that give the desired λ_s values are shown in Figure 2. The figure also shows several populations of transient sources, with a range of local rate densities and isotropic energies obtained from Murase & Bartos (2019). We see that long gamma-ray bursts are the only sources from which we may expect some detectable coincidences.

4. Archival Results

The ranking distribution for the archival data is shown in Figure 3, along with the simulated distribution from the scrambled data set used in Section 3.2 to obtain the FAR. The power of the combined data analysis can be seen in Figure 4, which shows the FAR for the HAWC-ANTARES coincidences versus the FAR for the HAWC events alone. As expected, the FAR for HAWC-only events is reduced by 4 orders of magnitude. The low FAR of coincidences makes it useful for follow-up searches in real time.

After performing the analysis on unscrambled data, we found three events that pass the 1-per-year FAR threshold in this period. These three events are summarized in Table 1. Although these events are rare given their FAR, they are still consistent with background as shown by the posttrials p-value(last column in Table 1, calculated as $p_{\mathrm{post-trials}} = 1 - \exp(-\mathrm{FAR} \cdot \Delta T)$, where ΔT is the live time of the analysis). Tables 2 and 3 have the information of the events that make the coincidences.

The sky maps of the coincidences are shown in Figure 5. Each sky map shows the position of the individual events along with their uncertainties, as well as the best position of the coincidence. Also shown are the sources of the fourth Fermi Large Area Telescope gamma-ray source Catalog (Abdollahi et al. 2020) that appear in each of the regions.

We searched for past activity around the coincidences by looking in the *Fermi* All-sky Variability Analysis (FAVA) online tool.[82] We did not find any past activity in the regions of the coincidences 2 and 3. For coincidence 1, the source J0144.6 +2705, associated with TXS 0141+268, is located 2.0° away from the position of the coincidence. FAVA reported a burst in 2018 from this source, which was found in the high-energy band (800 MeV–300 GeV).

A search in the SIMBAD Catalog (Wenger et al. 2000) revealed several sources inside the uncertainty regions of the positions of the coincidences. For coincidence 1, we found several quasars, along with a radio source and an X-ray source. All of the quasars have redshift measurements larger than 0.3, the farthest HAWC can observe before the gamma rays start to be severely attenuated by the extragalactic background light (Albert et al. 2021).

In coincidence 2, there were 115 sources inside the uncertainty region of the coincidence in the SIMBAD Catalog. Around 15 sources are stars, while the rest are galaxies.

For coincidence 3 in 2019, we found only eight sources in the SIMBAD catalog: three molecular clouds, two stars, two radio sources, and one X-ray source. No information about the distance for the radio sources or X-ray source was available.

These coincidences are examples where, if the analysis had been running in real time, a follow-up observation in another wavelength could have pinpointed any source that is flaring in the region.

4.1. Upper Limit

After observing three coincidences in 4.39 yr of data with a FAR of less than 1 per yr, we calculate the 90% confidence

[82] https://fermi.gsfc.nasa.gov/ssc/data/access/lat/FAVA/

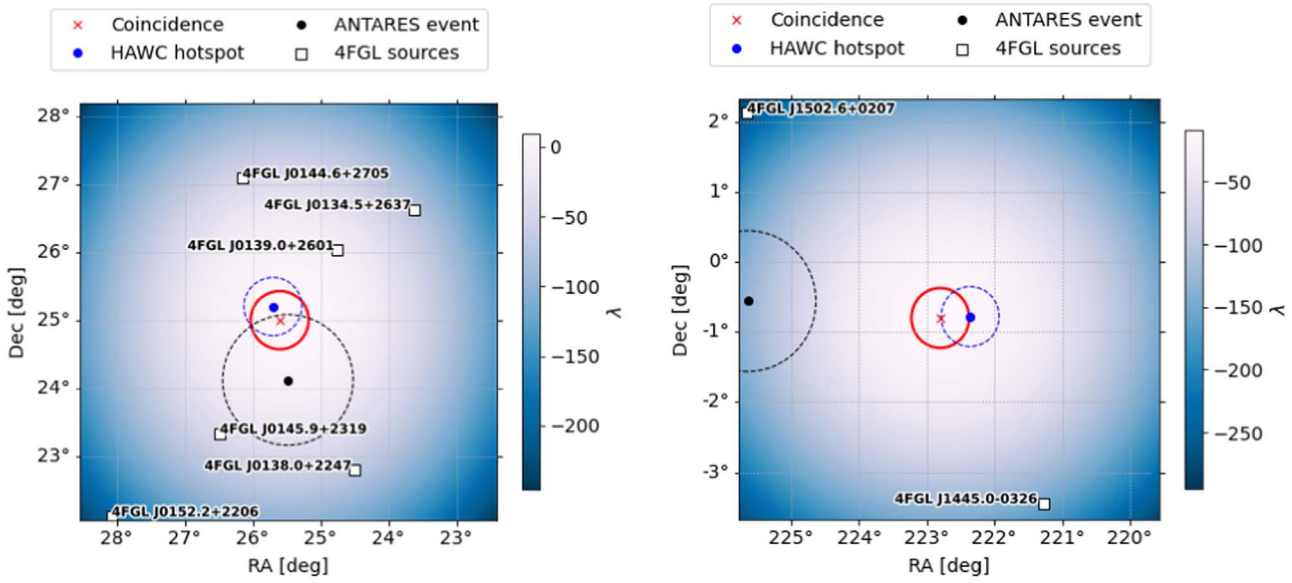

(a) Coincidence 1.

(b) Coincidence 2.

(c) Coincidence 3.

Figure 5. Sky maps in celestial coordinates of the HAWC-ANTARES coincidences with FAR values below one coincidence per year found in the archival data. The positions of the individual events are marked with both the dots. The best-fit combined positions $\boldsymbol{x}_{\rm coinc}$, found after optimizing $\lambda(\boldsymbol{x})$ (Equation (2)), are marked with a red cross. Circles represent the 50% containment regions.

level upper limit for the parameter space presented in Figure 2. Using Equation (9.54) from Cowan (2002), we obtain $\lambda_{\rm signal} = 3.85$. We apply the procedure of Section 3.3 to find the upper limit on the total isotropic equivalent neutrino energy as a function of the local source rate.

5. Conclusion

Archival data that span 2015 to 2020 were analyzed to search for multimessenger sources through a coincidence analysis between subthreshold data of the HAWC Observatory and public data from the ANTARES neutrino telescope. In this time period, three coincidences were found with a FAR of less than one coincidence per year. Although these coincidences are consistent with background expectations, they are still useful for follow-up observations since the FAR can be improved by several orders of magnitude, compared to when the events are coming from the individual detectors. It is possible that a flare in the region could have been observed by a follow-up telescope, hinting at the presence of a multimessenger source, if the analysis had been running in real time.

Furthermore, based on the sensitivity and discovery potential studies, we found that long gamma-ray bursts are potential candidates for a possible coincidence detection with this analysis. This work is also a proof of principle analysis for future neutrino observatories. In this sense, with the end of operations of ANTARES, we expect that this analysis will be

implemented for KM3NeT with an effective volume already exceeding ANTARES. Based on the information in Adrián-Martínez et al. (2016), a back-of-the-envelope estimate suggests an improvement of the sensitivity and discovery potential of more than 1 order of magnitude, assuming the same live time. We look forward to implementing this new stream within AMON.

AMON: This research or portions of this research were conducted with Advanced CyberInfrastructure computational resources provided by the Institute for Computational and Data Sciences at the Pennsylvania State University (https://www.icds.psu.edu/). This material is based upon work supported by the National Science Foundation under grants PHY-1708146 and PHY-1806854 and by the Institute for Gravitation and the Cosmos of the Pennsylvania State University. Any opinions, findings, and conclusions or recommendations expressed in this material are those of the author(s) and do not necessarily reflect the views of the National Science Foundation.

ANTARES: The authors acknowledge the financial support of the funding agencies: Centre National de la Recherche Scientifique (CNRS), Commissariat à l'énergie atomique et aux énergies alternatives (CEA), Commission Européenne (FEDER fund and Marie Curie Program), Institut Universitaire de France (IUF), LabEx UnivEarthS (ANR-10-LABX-0023 and ANR-18-IDEX-0001), Région Île-de-France (DIM-ACAV), Région Alsace (contrat CPER), Région Provence-Alpes-Côte d'Azur, Département du Var and Ville de La Seyne-sur-Mer, France; Bundesministerium für Bildung und Forschung (BMBF), Germany; Istituto Nazionale di Fisica Nucleare (INFN), Italy; Nederlandse organisatie voor Wetenschappelijk Onderzoek (NWO), the Netherlands; Executive Unit for Financing Higher Education, Research, Development and Innovation (UEFISCDI), Romania; Ministerio de Ciencia, Innovación, Investigación y Universidades (MCIU): Programa Estatal de Generación de Conocimiento (refs. PGC2018-096663-B-C41, -A-C42, -B-C43, -B-C44 and refs. PID2021-124591NB-C41, -C42, -C43) (MCIU/FEDER), Generalitat Valenciana: Prometeo (PROMETEO/2020/019), Grisolía (refs. GRISOLIA/2018/119, /2021/192) and GenT (refs. /2019/043, /2020/049, /2021/023) programs, Junta de Andalucía (ref. A-FQM-053-UGR18), La Caixa Foundation (ref. LCF/BQ/IN17/11620019), EU: MSC program (ref. 101025085), Spain; Ministry of Higher Education, Scientific Research and Innovation, Morocco; and the Arab Fund for Economic and Social Development, Kuwait. We also acknowledge the technical support of Ifremer, AIM and Foselev Marine for the sea operation and the CC-IN2P3 for the computing facilities.

HAWC: We acknowledge the support from: the US National Science Foundation (NSF); the US Department of Energy Office of High-Energy Physics; the Laboratory Directed Research and Development (LDRD) program of Los Alamos National Laboratory; Consejo Nacional de Ciencia y Tecnología (CONACyT), México, grants 271051, 232656, 260378, 179588, 254964, 258865, 243290, 132197, A1-S-46288, A1-S-22784, cátedras 873, 1563, 341, 323, Red HAWC, México; DGAPA-UNAM grants IG101320, IN111716-3, IN111419, IA102019, IN110621, IN110521; VIEP-BUAP; PIFI 2012, 2013, PROFOCIE 2014, 2015; the University of Wisconsin Alumni Research Foundation; the Institute of Geophysics, Planetary Physics, and Signatures at Los Alamos National Laboratory; Polish Science Centre grant, DEC-2017/27/B/ST9/02272; Coordinación de la Investigación Científica de la Universidad Michoacana; Royal Society—Newton Advanced Fellowship 180385; Generalitat Valenciana, grant CIDEGENT/2018/034; The Program Management Unit for Human Resources & Institutional Development, Research and Innovation, NXPO (grant No. B16F630069); Coordinación General Académica e Innovación (CGAI-UdeG), PRODEP-SEP UDG-CA-499; Institute of Cosmic Ray Research (ICRR), University of Tokyo. H.F. acknowledges support by NASA under award number 80GSFC21M0002. We also acknowledge the significant contributions over many years of Stefan Westerhoff, Gaurang Yodh, and Arnulfo Zepeda Dominguez, all deceased members of the HAWC collaboration. Thanks to Scott Delay, Luciano Díaz, and Eduardo Murrieta for technical support.

Facilities: HAWC, ANTARES, AMON.

Software: astropy (Price-Whelan et al. 2018), FIRESONG (Taboada et al. 2017), numpy (Van der Walt et al. 2011), scipy (Virtanen et al. 2020) matplotlib (Hunter 2007), pandas (McKinney 2010), amonpy (Ayala Solares et al. 2020).

ORCID iDs

H. A. Ayala Solares https://orcid.org/0000-0002-2084-5049
S. Coutu https://orcid.org/0000-0003-2923-2246
D. Cowen https://orcid.org/0000-0003-4738-0787
D. B. Fox https://orcid.org/0000-0002-3714-672X
T. Grégoire https://orcid.org/0000-0001-8711-1456
F. McBride https://orcid.org/0000-0001-6191-1244
M. Mostafá https://orcid.org/0000-0002-7675-4656
K. Murase https://orcid.org/0000-0002-5358-5642
S. Wissel https://orcid.org/0000-0003-0569-6978
M. Ardid https://orcid.org/0000-0002-3199-594X
S. Ardid https://orcid.org/0000-0003-4821-6655
B. Baret https://orcid.org/0000-0001-6064-3858
B. Belhorma https://orcid.org/0000-0001-6064-3858
V. Bertin https://orcid.org/0000-0001-6688-4580
S. Biagi https://orcid.org/0000-0001-8598-0017
M. Bissinger https://orcid.org/0000-0002-8709-8236
A. Capone https://orcid.org/0000-0001-9657-6220
V. Carretero https://orcid.org/0000-0002-7540-0266
S. Celli https://orcid.org/0000-0002-7592-0851
M. Chabab https://orcid.org/0000-0002-2772-4290
T. Chiarusi https://orcid.org/0000-0001-8454-8644
J. A. B. Coelho https://orcid.org/0000-0001-5615-3899
C. Distefano https://orcid.org/0000-0001-8632-1136
I. Di Palma https://orcid.org/0000-0003-1544-8943
D. Dornic https://orcid.org/0000-0001-5729-1468
P. Fermani https://orcid.org/0000-0003-1204-4097
K. Graf https://orcid.org/0000-0002-1921-5568
H. van Haren https://orcid.org/0000-0001-8041-8121
J. Hofestädt https://orcid.org/0000-0002-7848-117X
O. Kalekin https://orcid.org/0000-0001-6206-1288
U. Katz https://orcid.org/0000-0002-7063-4418
A. Kouchner https://orcid.org/0000-0001-7068-2113
M. Lamoureux https://orcid.org/0000-0002-8860-5826
S. Navas https://orcid.org/0000-0003-1688-5758
T. Pradier https://orcid.org/0000-0001-5501-0060
A. Romanov https://orcid.org/0000-0001-5952-2370
J. Schnabel https://orcid.org/0000-0003-1233-7738
F. Schüssler https://orcid.org/0000-0003-1500-6571
M. Spurio https://orcid.org/0000-0002-8698-3655
Th. Stolarczyk https://orcid.org/0000-0002-0551-7581

B. Vallage https://orcid.org/0000-0003-1255-8506
V. Van Elewyck https://orcid.org/0000-0002-8242-5453
A. Zegarelli https://orcid.org/0000-0003-1497-3826
J. D. Zornoza https://orcid.org/0000-0002-1834-0690
J. Zúñiga https://orcid.org/0000-0002-1041-6451
A. Albert https://orcid.org/0000-0003-0197-5646
R. Babu https://orcid.org/0000-0002-5529-6780
E. Belmont-Moreno https://orcid.org/0000-0003-3207-105X
K. S. Caballero-Mora https://orcid.org/0000-0002-4042-3855
T. Capistrán https://orcid.org/0000-0003-2158-2292
A. Carramiñana https://orcid.org/0000-0002-8553-3302
S. Casanova https://orcid.org/0000-0002-6144-9122
U. Cotti https://orcid.org/0000-0002-7607-9582
J. Cotzomi https://orcid.org/0000-0002-1132-871X
S. Coutiño de León https://orcid.org/0000-0002-7747-754X
E. De la Fuente https://orcid.org/0000-0001-9643-4134
C. de León https://orcid.org/0000-0002-8528-9573
M. A. DuVernois https://orcid.org/0000-0002-2987-9691
M. Durocher https://orcid.org/0000-0003-2169-0306
J. C. Díaz-Vélez https://orcid.org/0000-0002-0087-0693
K. Engel https://orcid.org/0000-0001-5737-1820
C. Espinoza https://orcid.org/0000-0001-7074-1726
K. L. Fan https://orcid.org/0000-0002-8246-4751
M. Fernández Alonso https://orcid.org/0000-0002-6305-3009
N. Fraija https://orcid.org/0000-0002-0173-6453
J. A. García-González https://orcid.org/0000-0002-4188-5584
F. Garfias https://orcid.org/0000-0003-1122-4168
M. M. González https://orcid.org/0000-0002-5209-5641
J. A. Goodman https://orcid.org/0000-0002-9790-1299
J. P. Harding https://orcid.org/0000-0001-9844-2648
D. Huang https://orcid.org/0000-0002-3808-4639
F. Hueyotl-Zahuantitla https://orcid.org/0000-0002-5527-7141
P. Hüntemeyer https://orcid.org/0000-0002-3302-7897
A. Iriarte https://orcid.org/0000-0001-5811-5167
V. Joshi https://orcid.org/0000-0003-4467-3621
A. Lara https://orcid.org/0000-0001-6336-5291
H. León Vargas https://orcid.org/0000-0001-5516-4975
J. T. Linnemann https://orcid.org/0000-0003-2696-947X
A. L. Longinotti https://orcid.org/0000-0001-8825-3624
G. Luis-Raya https://orcid.org/0000-0003-2810-4867
K. Malone https://orcid.org/0000-0001-8088-400X
O. Martinez https://orcid.org/0000-0001-9052-856X
I. Martinez-Castellanos https://orcid.org/0000-0001-9035-1290
J. Martínez-Castro https://orcid.org/0000-0002-2824-3544
J. A. Matthews https://orcid.org/0000-0002-2610-863X
P. Miranda-Romagnoli https://orcid.org/0000-0002-8390-9011
J. A. Morales-Soto https://orcid.org/0000-0001-9361-0147
E. Moreno https://orcid.org/0000-0002-1114-2640
L. Nellen https://orcid.org/0000-0003-1059-8731
M. U. Nisa https://orcid.org/0000-0002-6859-3944
R. Noriega-Papaqui https://orcid.org/0000-0001-7099-108X
E. G. Pérez-Pérez https://orcid.org/0000-0001-5998-4938
C. D. Rho https://orcid.org/0000-0002-6524-9769
D. Rosa-González https://orcid.org/0000-0003-1327-0838
F. Salesa Greus https://orcid.org/0000-0002-8610-8703
A. Sandoval https://orcid.org/0000-0001-6079-2722
M. Schneider https://orcid.org/0000-0001-8644-4734
A. J. Smith https://orcid.org/0000-0002-1012-0431
R. W. Springer https://orcid.org/0000-0002-1492-0380
K. Tollefson https://orcid.org/0000-0001-9725-1479
I. Torres https://orcid.org/0000-0002-1689-3945
R. Torres-Escobedo https://orcid.org/0000-0002-7102-3352
F. Ureña-Mena https://orcid.org/0000-0002-2748-2527
K. Whitaker https://orcid.org/0000-0001-7160-3632
E. Willox https://orcid.org/0000-0002-6623-0277
A. Zepeda https://orcid.org/0000-0001-9976-2387
H. Zhou https://orcid.org/0000-0003-0513-3841

References

Abdollahi, S., Acero, F., Ackermann, M., et al. 2020, ApJS, 247, 33
Abeysekara, A. U., Albert, A., Alfaro, R., et al. 2017, ApJ, 843, 39
Adrián-Martínez, S., Ageron, M., Aharonian, F., et al. 2016, JPhG, 43, 084001
Ageron, M., Aguilar, J., Al Samarai, I., et al. 2011, NIMPA, 656, 11
Ahlers, M., & Murase, K. 2014, PhRvD, 90, 023010
Albert, A., Alfaro, R., Alvarez, C., et al. 2020, ApJ, 905, 76
Albert, A., Alvarez, C., Camacho, J. R. A., et al. 2021, ApJ, 907, 67
Albert, A., André, M., Anghinolfi, M., et al. 2017, PhRvD, 96, 082001
Albert, A., André, M., Anghinolfi, M., et al. 2018, ApJL, 863, L30
Ayala Solares, H. A., Coutu, S., Cowen, D., et al. 2020, APh, 114, 68
Ayala Solares, H. A., Cowen, D. F., DeLaunay, J. J., et al. 2019, ApJ, 886, 98
Ayala Solares, et al. 2021, ApJ, 906, 63
Chang, P., Allen, G., Anderson, W., et al. 2019, BAAS, 51, 436
Cowan, G. 2002, Statistical Data Analysis (Oxford: Oxford Univ. Press)
Domínguez, A., Primack, J. R., Rosario, D. J., et al. 2011, MNRAS, 410, 2556
Fisher, R. A. 1938, Statistical Methods for Research Workers (Edinburgh: Oliver and Boyd)
Hunter, J. 2007, CSE, 9, 90
Illuminati, G., Aublin, J., & Navas, S. 2019, ICRC (Madison, WI), 36, 920
McKinney, W. 2010, in Proc. of the 9th Python in Science Conf., ed. S. van der Walt & J. Millman, 56
Murase, K., & Bartos, I. 2019, ARNPS, 69, 477
Price-Whelan, A. M., Sipőcz, B. M., Günther, H. M., et al. 2018, AJ, 156, 123
Strolger, L.-G., Dahlen, T., Rodney, S. A., et al. 2015, ApJ, 813, 93
Taboada, I., Tung, C. F., & Wood, J. 2017, ICRC (Busan), 301, 663
Turley, C. F., Fox, D. B., Keivani, A., et al. 2018, ApJ, 863, 64
Van der Walt, S., Colbert, S. C., & Varoquaux, G. 2011, CSE, 13, 22
Virtanen, P., Gommers, R., Oliphant, T. E., et al. 2020, NatMe, 17, 261
Wenger, M., Ochsenbein, F., Egret, D., et al. 2000, AAPS, 143, 9